

Distributed Biasing of Differential RF Circuits

Wael M. Fathelbab, *Member, IEEE*, and Michael B. Steer, *Fellow, IEEE*

Abstract—A distributed balun is presented as an alternative to inductor-based biasing of active differential circuits. The new scheme has broad bandwidth with low loss and is suited to broad-band multifunctional RF and microwave circuits. Additionally, the distributed biasing circuit discriminates between differential and common-mode signals leading to high common-mode rejection. Measured gains, centered at 580 MHz, of a selected pseudodifferential amplifier using the new biasing circuit confirm the underlying theory.

Index Terms—Balun, broad-band biasing, differential amplifier.

I. INTRODUCTION

RADIO-FREQUENCY (RF) circuits commonly utilize differential signal paths with the benefit of noise immunity and reduced sensitivity to component variations. On-chip RF power amplifiers are often pseudodifferential where the common current source typically used in fully differential circuits is sacrificed to enable a larger voltage swing (see Fig. 1). Here, the inductors present high RF impedance to the transistors (represented as transconductances), while providing a low-impedance path for bias currents. With a sufficiently high- Q inductor, RF energy is delivered to the load rather than being dissipated in the bias circuitry. With the relatively low Q of on-chip planar inductors [1], inductance peaking near self-resonance is utilized and this leads to narrow-band operation. Thus, in critical situations, off-chip inductors are sometimes used in conjunction with on-chip active devices. In addition, inductive biasing of pseudodifferential circuits presents the same environment to common- and differential-mode signals so that the common-mode rejection ratio (CMRR) is one.

This paper presents a biasing scheme for broad-band pseudodifferential circuits leading to high CMRR. The biasing circuitry consists of a coupled-line structure analogous to that of a Marchand balun [2] (see Fig. 2). The balun structure is comprised of transmission lines connected to a pair of coupled lines that normally transforms a single-ended impedance at port 1 to a balanced output at ports 3 and 4. The capacitors in Fig. 2 are purely for miniaturization purposes [3], [4] since the distributed transmission lines are quarter-wavelength long at a frequency well above the passband of the balun. In Section II, the validity of the Marchand balun structure as a biasing circuit is investigated and analysis of the even- and odd-mode impedances of

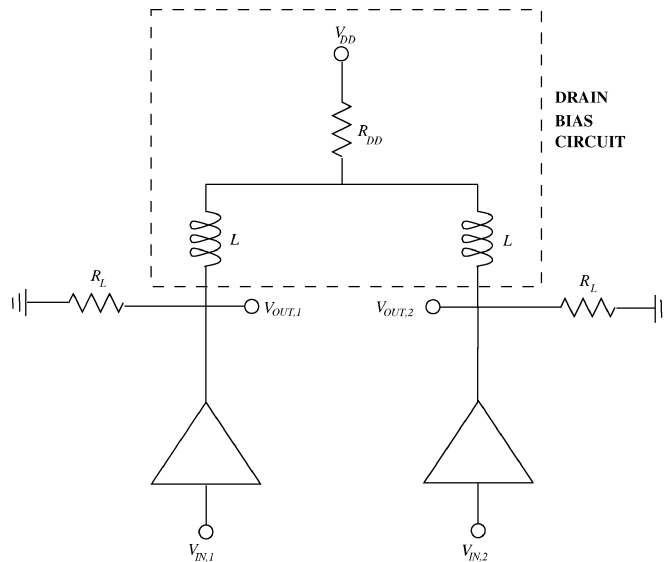


Fig. 1. Pseudodifferential circuit without a constant-current source, bias inductors L at the drains, parasitic supply resistance R_{DD} , and single-ended load impedance R_L .

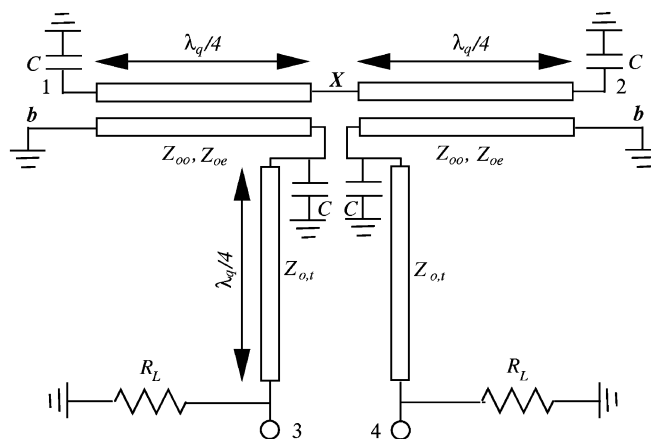


Fig. 2. Marchand balun-like biasing circuit with single-ended load resistance R_L (dc bias may be applied at ports b using decoupling capacitors).

the balanced ports is presented. Practical implementations are presented in Section III.

II. ANALYSIS AND DESIGN

Here, the design equations of a class of distributed differential biasing circuits are developed based on coupled resonator theory. In Section II-A, the equations describing the CMRR are first developed, as maximizing the CMRR in pseudodifferential circuits is a key design objective. The subsequent design equations enable the design of the biasing-circuit network with specified characteristics.

Manuscript received November 28, 2003. This work was supported by the U.S. Army Research Office as a Multidisciplinary University Research Initiative on Multifunctional Adaptive Radio Radar and Sensors under Grant DAAD19-01-1-0496.

The authors are with the Department of Electrical and Computer Engineering, North Carolina State University, Raleigh, NC 27695-7911 USA.

Digital Object Identifier 10.1109/TMTT.2004.827048

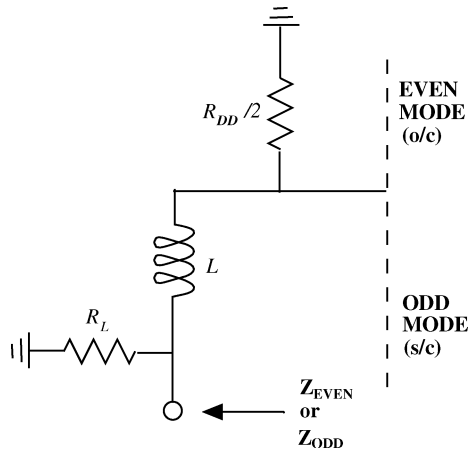


Fig. 3. Modal sub-circuits of the inductor-based biasing circuit of Fig. 1 including single-ended load resistance R_L .

A. Conventional Biasing

Multifunctional systems require broad-band circuits and, for differential circuits, this requires large differential gain A_d . At the same time, it is desirable to minimize the common-mode gain A_c , as the resulting high CMRR provides immunity to substrate induced noise. With transistor transconductance g_m , and total even- and odd-mode impedances Z_{EVEN} and Z_{ODD} presented to the drains of the transistors, the gains are approximately

$$A_d = g_m Z_{ODD} \text{ and } A_c = g_m Z_{EVEN} \quad (1)$$

and, thus,

$$\text{CMRR} = \frac{A_d}{A_c} = \frac{Z_{ODD}}{Z_{EVEN}}. \quad (2)$$

Thus, the desired amplifier characteristics are obtained by synthesizing the even- and odd-mode impedances.

Modal analysis of the inductor biasing circuit results in Fig. 3, from which the total even-mode impedance is

$$Z_{EVEN}(s) = \left(sL + \frac{R_{DD}}{2} \right) // R_L \quad (3)$$

where s is the Laplace operator ($//$ indicates a parallel connection) and the total odd-mode impedance is

$$Z_{ODD}(s) = sL // R_L. \quad (4)$$

Thus, unless the inductance is very large, there will be a strong frequency variation of Z_{ODD} and Z_{EVEN} . Since R_{DD} is often negligible, the CMRR is also one. In the differential-mode, the gain is maximized over a broad frequency band for a specific single-ended load impedance R_L . However, if the common-mode gain has prescribed frequency characteristics, then the CMRR will be inversely proportional to the even-mode impedance. Thus, low even-mode impedance of the biasing network is desirable, as this suppresses common-mode noise. This defines a vital design objective of the new biasing circuit.

B. New Design Based on Analogy to Coupled Resonators

Coupled resonator structures are appropriate topology choices that present different impedances for the common-

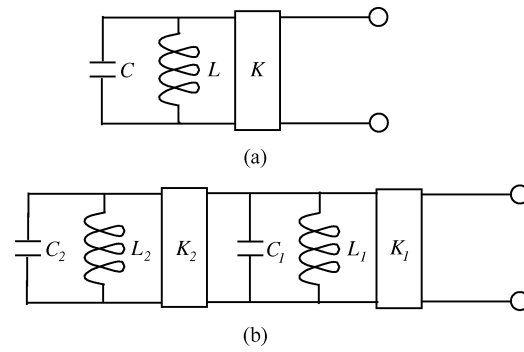


Fig. 4. Coupled lumped-element bandpass resonators. (a) Single resonator coupled into by an inverter. (b) Pair of resonators coupled by inverters.

and differential-mode signals. In essence, bias is also a common-mode signal and must be accommodated in the chosen topology. A class of appropriate topologies is based on a lumped bandpass resonator coupled into by the inverter K , shown in Fig. 4(a). The inverter element is an idealized component that is independent of frequency and can be approximated by a quarter-wavelength-long transmission line, as well as by various other circuit configurations [5]. At resonance, the bandpass resonator presents an open circuit and, following impedance inversion, the input impedance of the network is a short circuit. This is then the kind of network required to be presented to the common-mode signals. The second part of the network synthesis problem is a creation of the high-impedance condition for differential-mode signals. Again, we will consider this issue separately. Fig. 4(b) illustrates a pair of bandpass resonators coupled by inverters. At resonance, the input impedance of the network is infinite. This is because the high impedance of resonator 2 transforms to a short circuit after the second inverter K_2 , and this subsequently appears as an open circuit at the input of the network. Thus, by adding an extra resonator, another topology suitable for the differential-mode operation is derived. If a load is now connected in parallel with this network, then at resonance, this will be the total impedance presented to the output transistors of the pseudodifferential amplifier. In summary, presenting different impedances for common- and differential-mode signals is desired. It is shown in Section II-C that the Marchand balun structure has the requisite properties.

C. Distributed Biasing

Consider now the topology of the Marchand balun of Fig. 2 with the balanced ports 3 and 4 connected to the output of the pseudodifferential circuit. The aim here is to show that this topology has the requisite even- and odd-mode impedances. Performing modal analysis at the balanced ports, the modal sub-networks of Fig. 5 are obtained. In analyzing this structure, we shall make use of the network model of pair of coupled lines in a homogeneous media [6] (shown in Fig. 6). Direct application of the network model and application of the relevant port conditions, dictated by the modal sub-networks of the biasing circuit at point X, simplifies the equivalent sub-networks of Fig. 5 to those of Fig. 7. Application of the relevant Kuroda transformation [5] to distribute the inductance in Fig. 7(c) results in the transformed sub-circuits of Fig. 7(d). Scrutiny in

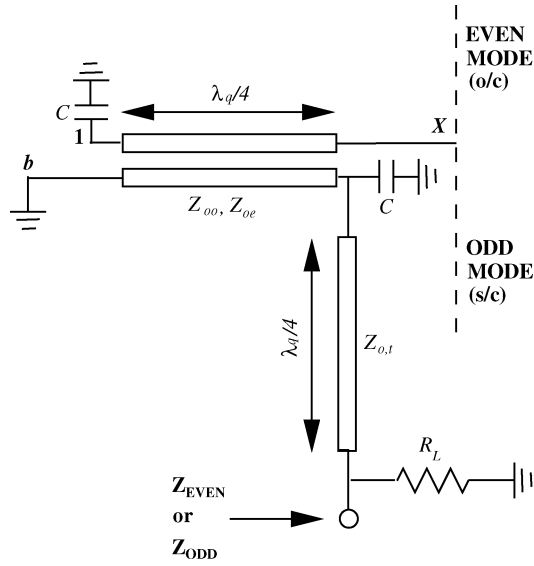


Fig. 5. Modal sub-networks of the balun-like biasing circuit of Fig. 2 with single-ended load resistance R_L (assuming negligible power supply source impedance R_{DD}).

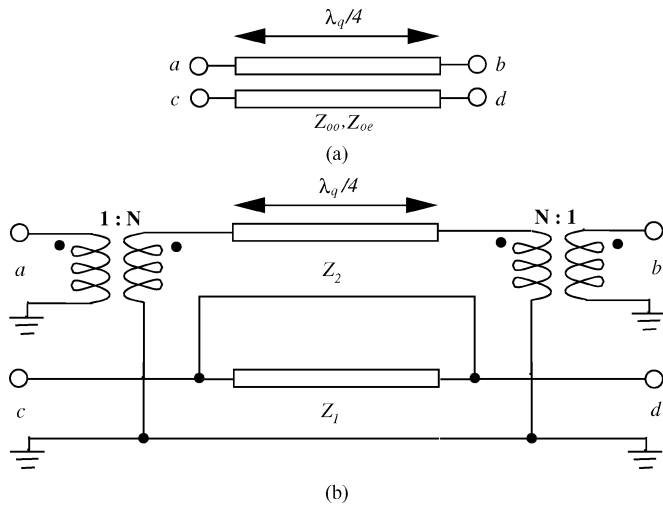


Fig. 6. Pair of symmetrical coupled lines in homogenous media. (a) Physical layout. (b) Equivalent-network model with $N = (Z_{oe} + Z_{oo}) / (Z_{oe} - Z_{oo})$.

Fig. 7(b) and (d) reveals that they are, in fact, analogous to the lumped-element coupled resonator examples discussed earlier. The major differences are that the transmission lines replace the inverters and the additional resistor R_c represents the loss associated with each capacitor. In the distributed domain, each inductor or capacitor also represents a short- or open-circuited stub, respectively, which is a quarter-wavelength long at the frequency f_q . The open-circuited stubs may, however, be approximated by lumped capacitors for miniaturization purposes. Thus, over the operating band, the performance of the even- and odd-mode sub-circuits is very close to their lumped-element counterparts. In summary, centered at a frequency f_o , the structure of the Marchand balun maximizes differential power delivery to the load while minimizing the gain of common-mode signals. DC bias may easily be applied through the short-circuited ports (labeled b in Fig. 2) with the usage of decoupling capacitors. The mathematical formulations

for the total even- and odd-mode impedances with lumped capacitors are derived from Fig. 7(b) and (c) as follows:

$$Z_{\text{EVEN}}(S) = \frac{N_1 S^2 + N_2 S}{D_1 S^2 + D_2 S + D_3} \quad (5)$$

with coefficients

$$\begin{aligned} N_1 &= j(2Z_{ot}^2 Z_1 \pi f C R_L) \\ N_2 &= Z_1 R_L Z_{ot} + Z_{ot}^2 R_L \\ D_1 &= (Z_1 R_L) + j(2Z_{ot}^2 \pi f C Z_1) \\ D_2 &= (Z_{ot}^2 + Z_{ot} Z_1) + j(2Z_{ot} R_L \pi f C Z_1) \\ D_3 &= Z_{ot} R_L \end{aligned}$$

and

$$Z_{\text{ODD}}(S) = \frac{N_1 S^3 + N_2 S^2 + N_3 S}{D_1 S^3 + D_2 S^2 + D_3 S + D_4} \quad (6)$$

with coefficients

$$\begin{aligned} N_1 &= Z_{ot}^2 R_L Z_1 \\ N_2 &= j(2Z_2 Z_{ot}^2 R_L \pi f C Z_1) \\ N_3 &= Z_1 Z_2 Z_{ot} R_L + Z_2 Z_{ot}^2 R_L \\ D_1 &= Z_{ot}^2 Z_1 \\ D_2 &= (Z_1 Z_2 R_L + Z_1 Z_{ot} R_L) + j(2Z_2 Z_{ot}^2 \pi f C Z_1) \\ D_3 &= (Z_2 Z_{ot} Z_1 + Z_2 Z_{ot}^2) + j(2Z_2 Z_{ot} \pi f C Z_1 R_L) \\ D_4 &= Z_2 Z_{ot} R_L. \end{aligned}$$

In (5) and (6), S is the Richards transform [5] defined as $j \tan(\theta) = j \tan((\pi/2)(f/f_q))$, and f_q is the frequency at which the distributed lines of the balun are a quarter-wavelength long. In the above equations, Z_{ot} is the characteristic impedance of the uncoupled transmission lines, while

$$Z_1 = \frac{\sqrt{Z_{oe} Z_{oo}}}{\sqrt{1 - \left(\frac{Z_{oe} - Z_{oo}}{Z_{oe} + Z_{oo}}\right)^2}} \quad (7)$$

and

$$Z_2 = \sqrt{Z_{oe} Z_{oo}} \frac{\sqrt{1 - \left(\frac{Z_{oe} - Z_{oo}}{Z_{oe} + Z_{oo}}\right)^2}}{\left(\frac{Z_{oe} - Z_{oo}}{Z_{oe} + Z_{oo}}\right)^2} \quad (8)$$

with Z_{oe} and Z_{oo} being the even- and odd-mode impedances of the coupled lines forming the balun. The total even- and odd-mode impedances presented to the pseudodifferential active circuit are, in general, complex and, thus, may be written in the following notation:

$$|Z_{\text{EVEN}}(S)| = \sqrt{\Re\{Z_{\text{EVEN}}(S)\}^2 + \Im\{Z_{\text{EVEN}}(S)\}^2} \quad (9)$$

$$|Z_{\text{ODD}}(S)| = \sqrt{\Re\{Z_{\text{ODD}}(S)\}^2 + \Im\{Z_{\text{ODD}}(S)\}^2}. \quad (10)$$

Hence, the procedure of determining the circuit parameters of the new biasing circuit is fairly simple. Suitable choices of the characteristic impedances Z_1 and Z_2 solve (7) and (8) for the even- and odd-mode characteristic impedances Z_{oe} and Z_{oo} ,

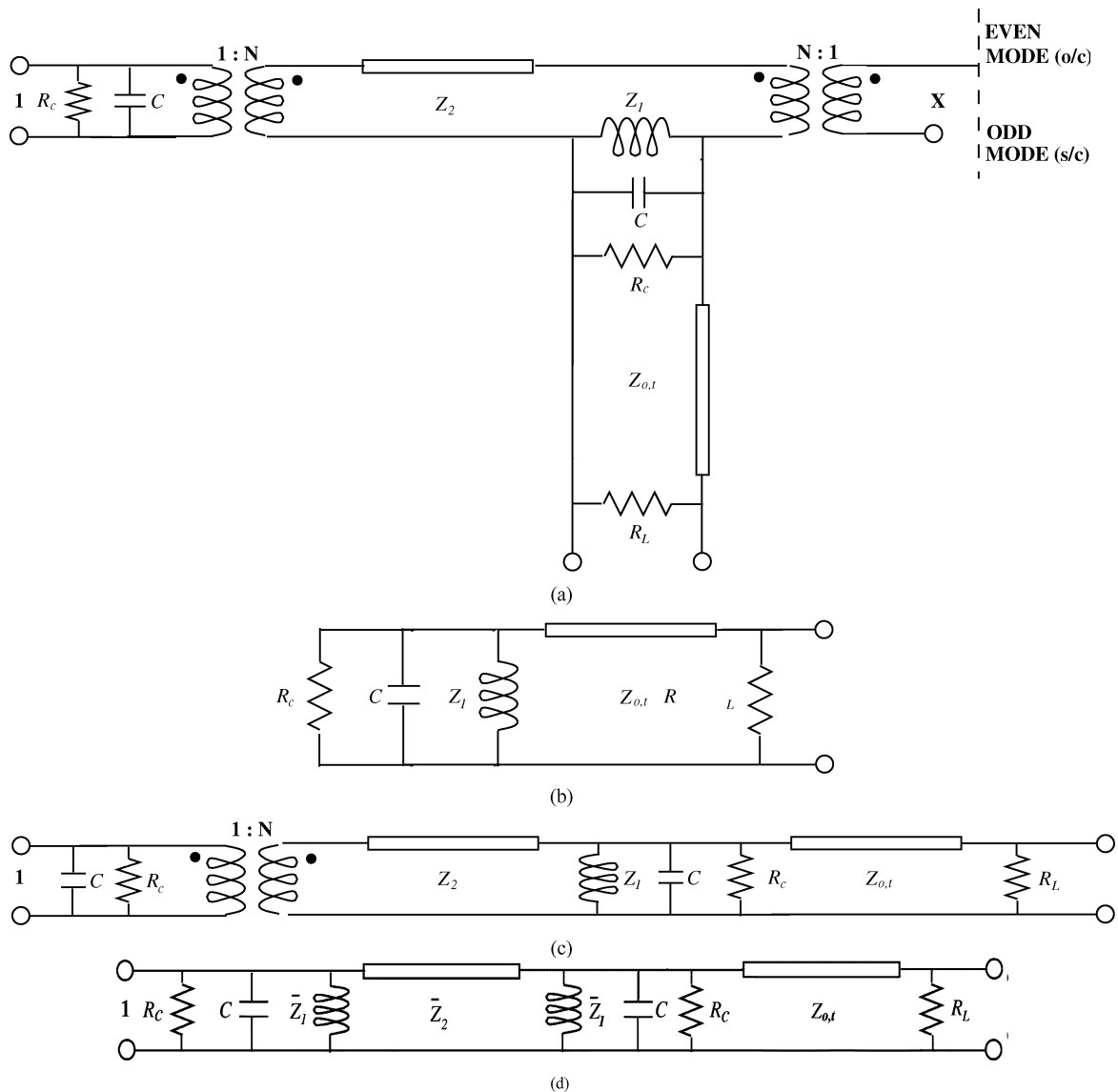


Fig. 7. Equivalent sub-circuits of Fig. 5: (a) utilizing the network model, (b) even-mode sub-circuit, (c) odd-mode sub-circuit, and (d) odd-mode sub-circuit after the Kuroda transformation with $\bar{Z}_1 = 1/Z_{oe}$ and $\bar{Z}_2 = (Z_{oe} - Z_{oo}) / (2Z_{oe}Z_{oo})$.

respectively. Selection of the characteristic line impedance Z_{ot} together with choice of capacitance value C fully determines (5) and (6). The magnitudes of the total even- and odd-mode impedance functions may then be evaluated using (9) and (10). The commensurate length of the transmission lines will be determined by the value of C . Zero capacitance results in the lines being a quarter-wavelength long at the center of the operating band, otherwise miniaturization of the lines is feasible. An example that shows the overall characteristics of the magnitudes of the even- and odd-mode impedances without lumped capacitors is depicted in Fig. 8 for a range of single-ended load resistances R_L .

D. Discriminative Operating Bandwidth

The operating bandwidth of the balun is defined at the crossover frequencies where

$$|Z_{\text{EVEN}}(S)| = |Z_{\text{ODD}}(S)|. \quad (11)$$

At the crossover frequency points (see Fig. 8), the CMRR of the pseudodifferential circuit is one and the balun has a similar performance to that of the nondiscriminative inductor-based biasing circuit. For a certain choice of circuit parameters, the frequency points at which the even- and odd-mode impedances crossover may be altered facilitating adjustment of the discriminative bandwidth. This is demonstrated in Fig. 9 through a set of examples using the design procedure described in Section II-C. It is worth emphasizing that the total even- or odd-mode impedance of (5) or (6) is the impedance of the input of the balun in parallel with the single-ended load resistance R_L . This implies that, in order for the pseudodifferential circuit to deliver its power to the load, it is necessary that the output signal at each arm sees the correct impedance. Of course, there will only be a perfect match at the center of the band (since the input balun impedance is then infinite), but not at the crossover frequency points. However, a slight mismatch will only degrade the transfer of power slightly and is, therefore, acceptable. Fig. 8 illustrates this argument for a 50- Ω system

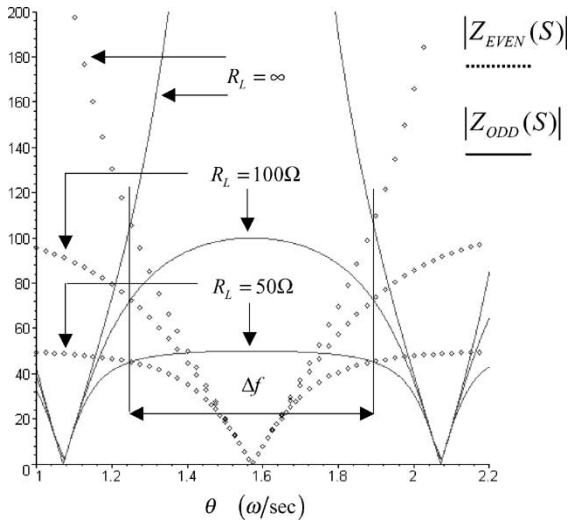


Fig. 8. Calculated magnitudes of the total even- and odd-impedances for a range of single-ended load resistances with circuit parameters $Z_{oe} = 208 \Omega$, $Z_{oo} = 51 \Omega$, $Z_{o,t} = 137 \Omega$, and $C = 0$ pF.

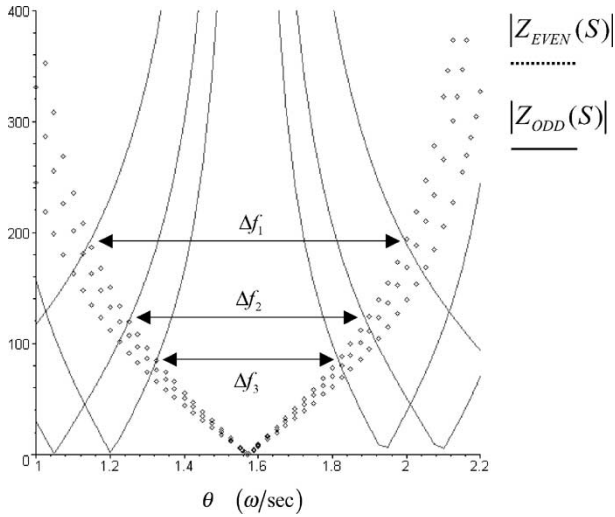


Fig. 9. Calculated magnitudes of the total even and odd impedances for an infinite single-ended load resistance R_L with the following circuit parameters: Δf_1 : $Z_{oe} = 157.32 \Omega$, $Z_{oo} = 58.45 \Omega$, $Z_{o,t} = 90 \Omega$, $C = 0$ pF, Δf_2 : $Z_{oe} = 205.36 \Omega$, $Z_{oo} = 47.82 \Omega$, $Z_{o,t} = 100 \Omega$, $C = 0$ pF, Δf_3 : $Z_{oe} = 307.26 \Omega$, $Z_{oo} = 22.24 \Omega$, $Z_{o,t} = 80 \Omega$, $C = 0$ pF.

for a particular choice of balun circuit parameters. In this example, the magnitudes of the total even- and odd-mode impedances at the crossover frequencies are approximately 43Ω . However, for a $100\text{-}\Omega$ system, it is obvious (see Fig. 8) that the impedance levels are much lower than 100Ω at the crossover frequencies, causing a big mismatch that need to be compensated for by adjusting the element values of the balun. Generally, the higher the system impedance, the higher the coupling required between the coupled lines of the balun.

E. Effect of Loss on Distributed Biasing

The remaining and most crucial design parameter to be discussed is the effect of loss of the transmission lines forming the distributed biasing circuit. The circuit Q will be affected by substrate and conductor losses, but mostly by the loss associated

with the lumped capacitors if circuit miniaturization is desired. Modification of the total even- and odd-mode impedances to take into account the effect of substrate, conductor, and capacitor loss R_c leads to

$$Z_{\text{EVEN}}(S) = \frac{N_1 S^2 + N_2 S}{D_1 S^2 + D_2 S + D_3} \quad (12)$$

with coefficients

$$\begin{aligned} N_1 &= (Z_{ot}^2 Z_1 R_L) + j(2Z_{ot}^2 Z_1 \pi f C R_L R_C) \\ N_2 &= Z_1 R_L Z_{ot} R_C + Z_{ot}^2 R_L R_C \\ D_1 &= (Z_1 R_L R_C + Z_{ot}^2 Z_1) + j(2Z_{ot}^2 \pi f C Z_1 R_C) \\ D_2 &= (Z_{ot}^2 R_C + Z_{ot} Z_1 R_C + Z_{ot} Z_1 R_L) \\ &\quad + j(2Z_{ot} R_L \pi f C Z_1 R_C) \\ D_3 &= Z_{ot} R_L R_C \end{aligned}$$

and

$$Z_{\text{ODD}}(S) = \frac{N_1 S^3 + N_2 S^2 + N_3 S}{D_1 S^3 + D_2 S^2 + D_3 S + D_4} \quad (13)$$

with coefficients

$$\begin{aligned} N_1 &= Z_{ot}^2 R_L Z_1 R_C \\ N_2 &= (R_L Z_2 Z_{ot}^2 Z_1) + j(2Z_2 Z_{ot}^2 R_L \pi f C Z_1 R_C) \\ N_3 &= Z_1 Z_2 Z_{ot} R_L R_C + Z_2 Z_{ot}^2 R_L R_C \\ D_1 &= Z_{ot}^2 Z_1 R_C \\ D_2 &= (Z_1 Z_2 R_L R_C + Z_1 Z_{ot} R_L R_C + Z_{ot}^2 Z_1 Z_2) \\ &\quad + j(2Z_2 Z_{ot}^2 \pi f C Z_1 R_C) \\ D_3 &= (Z_2 Z_{ot} Z_1 R_C + Z_2 Z_{ot}^2 R_C + Z_1 Z_2 Z_{ot} R_L) \\ &\quad + j(2Z_2 Z_{ot} \pi f C Z_1 R_L R_C) \\ D_4 &= Z_2 Z_{ot} R_L R_C. \end{aligned}$$

Now S is the general Richards transform [7], defined as $\tanh(\alpha + j\theta) = \tanh(\alpha + j(\pi/2)(f/f_q))$ and α is the attenuation constant in nepers/meter. With no miniaturization capacitors (i.e., $C = 0$, $R_c = \infty$) and a finite value of α , the same circuit parameters that generated the plots of Fig. 8 are now fed back into the modified equations (12) and (13) from which their magnitudes are evaluated using (9) and (10). Fig. 10 highlights the effect of parasitic loss present. This plot assumes infinite single-ended load impedance, i.e., it represents the input impedances of the balun itself. The effect of loss manifests itself as a degradation of the magnitudes of the even- and odd-mode impedance levels. At resonance, the odd-mode impedance is very high, but finite, and likewise, the opposite is true for the even-mode impedance. These impedances, in parallel with the single-ended load impedance, directly impact the achievable CMRR of the system and also lower the differential power transfer to the next stage. However, the plots of Fig. 10 assumed no capacitors for miniaturization purposes. Normally lumped capacitors will possess finite Q that will further deteriorate the CMRR and reduce power delivery to the next stage. This point is demonstrated by measurements in Section III.

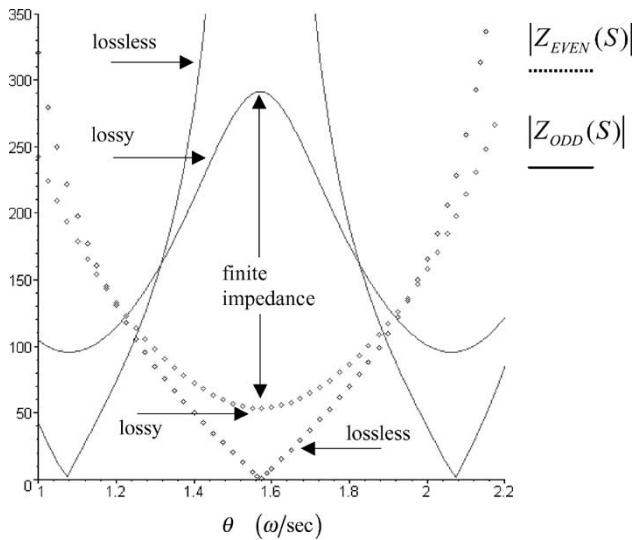


Fig. 10. Calculated magnitudes of lossy even and odd impedances for an infinite single-ended load resistance R_L with circuit parameters $Z_{oe} = 208 \Omega$, $Z_{oo} = 51 \Omega$, $Z_{o,t} = 137 \Omega$, $C = 0$ pF, and $\alpha = 0.2$ N/m.

III. EXPERIMENTAL RESULTS

A balanced power amplifier (HELA-10B) from Mini-Circuits,¹ with a gain of 10 dB was selected for experimental proof of principal. The chip is powered by a single +12-V dc power supply via a pair of external lumped inductors and consists of a pair of amplifiers in a pseudodifferential amplifier configuration. As the amplifiers are on the same chip, their gains and phase are well matched. The amplifier has an excellent second-order intercept of 88 dBm and is suitable for broad-band operation from 50 MHz to 1 GHz in a 50- Ω system. A number of distributed biasing circuits were implemented and integrated with the pseudodifferential amplifier. The design objective was to achieve broad-band bandwidth of 1.5:1 high odd-mode and low even-mode RF bias circuit impedances.

A. Conventional Biasing

The amplifier was tested first with the conventional inductor-based biasing circuit. A pair of high- Q lumped inductors of value 0.75 μ H was used and the circuit tested in both the differential and common modes. The measured common- and differential-mode gains are 10 and 9.5 dB, respectively, as shown in Fig. 11(a). The 0.75- μ H inductors present very high reactance of approximately 2.3 k Ω , at the center of the band. The inductor values chosen in this example contrast what can be achieved on an RF integrated circuit (RFIC) due to the lower achievable values of spiral inductors and their inherent narrow-band operation due to the self-resonant restraint. However, Fig. 11(a) demonstrates the most vital point about the nondiscriminatory bandwidth produced using the conventional inductor-based biasing scheme.

B. Distributed Biasing Without Miniaturization Capacitors

To verify the properties of the new biasing circuit, the Marchand balun structure with a center frequency of 580 MHz was designed. The optimized balun parameters are $Z_{oe} = 208 \Omega$,

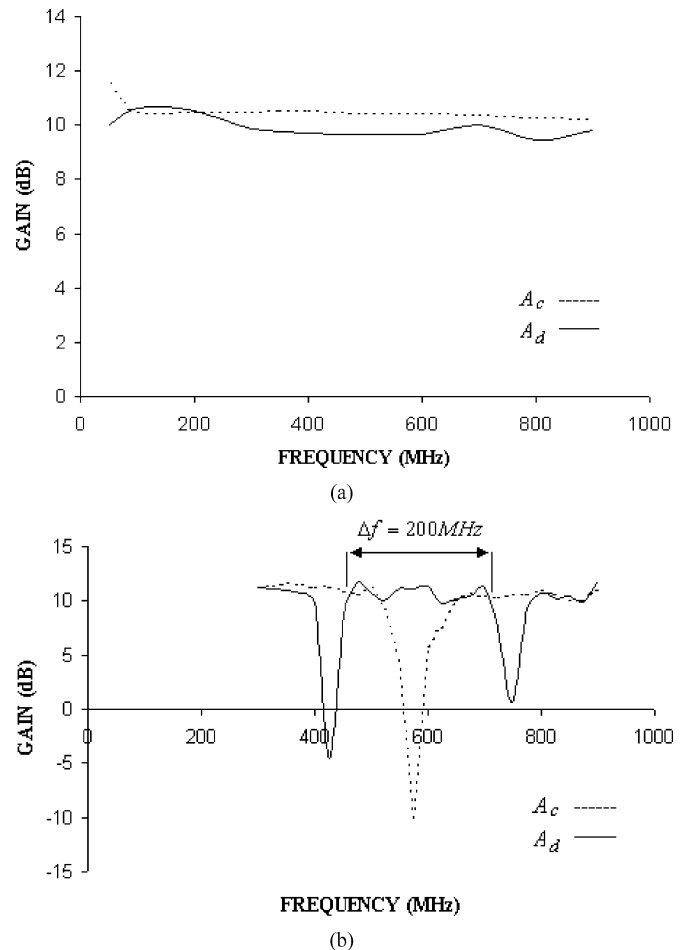


Fig. 11. Measured common-mode gain A_c and differential-mode gain A_d : (a) with an inductor-based biasing circuit with lumped inductors of 75 μ H and (b) with a balun-like biasing circuit without lumped capacitors with circuit parameters $Z_{oe} = 208 \Omega$, $Z_{oo} = 51 \Omega$, $Z_{o,t} = 137 \Omega$, and $\tan \delta = 0.016$.

$Z_{oo} = 51 \Omega$, $Z_{o,t} = 137 \Omega$, and $C = 0$ pF. The even- and odd-mode impedances were calculated based on a choice of $Z_1 = 129.5 \Omega$ and $Z_2 = 222.92 \Omega$ from (5)–(10). By referring to Fig. 8, it is seen that when the single-ended load impedance is 50 Ω , the magnitude of the total odd-mode impedance is desirably flat over the specific frequency band. This represents optimum power transfer to the load in a 50- Ω system. The HELA-10B chip was integrated with the balun on an FR4 printed circuit board with a substrate thickness of 6.2 mil (0.157 mm), relative dielectric constant of 4.7, and loss tangent of 0.016. The above impedances were then converted into physical dimensions using a commercial computer-aided design (CAD) tool² and the final circuit optimized. The resulting coupled lines were found to be 7-mil (0.177 mm) wide, 7-mil apart, and 3031-mil long. The transmission lines connecting the output ports of the RF chip to the coupled lines were 7-mil thick and 3031-mil long. The differential- and common-mode gains are shown in Fig. 11(b). While the differential-mode gain measured over 10 dB over a flat part of the band, the common-mode gain dipped to -10 dB at the expected resonant frequency. Thus, the device now differentiates between the common- and differential-mode signals over part of the operating bandwidth.

¹Mini-Circuits HELA-10B, 50-MHz–1-GHz amplifier.

²Advanced Design System (ADS), Agilent Technol., Palo Alto, CA, 2003.

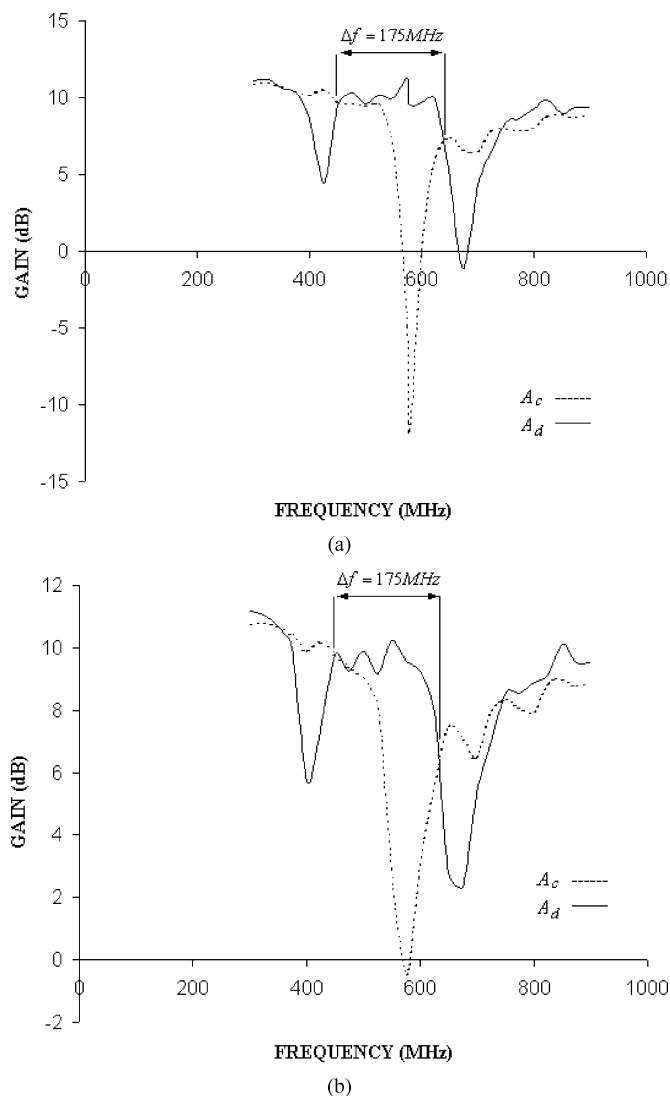


Fig. 12. Measured common-mode gain A_c and differential-mode gain A_d : (a) with a miniaturized balun-like biasing circuit using high- Q lumped capacitors with circuit parameters $Z_{oe} = 208 \Omega$, $Z_{oo} = 51 \Omega$, $Z_{o,t} = 137 \Omega$, $C = 5.6$ pF, $R_c = \infty$, and $\tan \delta = 0.016$ and (b) with miniaturized balun-like biasing circuit using high- Q lumped capacitors loaded with resistors with circuit parameters $Z_{oe} = 208 \Omega$, $Z_{oo} = 51 \Omega$, $Z_{o,t} = 137 \Omega$, $C = 5.6$ pF, $R_c = 1.2$ k Ω , and $\tan \delta = 0.016$.

The measured bandwidth, defined as $(\Delta f/f_o)$, is 34% of the resonant frequency 580 MHz, i.e., 1.4 : 1 bandwidth.

C. Distributed Biasing With Miniaturization Capacitors

Another design with the same layout dimensions as in (B) was implemented still operating at 580 MHz. The transmission lines were resonant at $3 \times 580 = 1740$ MHz. This yields a reduction in overall size by a factor of three with $C = 5.6$ pF. In Fig. 12(a), the measured response (with high- Q capacitors: $Q \approx 400$) is depicted. It is worth investigating the effect of loading the capacitors with resistors, as this drops their Q s. This was done with the thought in mind that the lumped capacitors could be replaced using tunable components to improve overall system functionality. Thin-film barium strontium titanate (BST) capacitors has recently shown great promise for the construction of high-frequency microwave components [8]. The Q of an

on-chip BST capacitor ranges from 30 to 40. Fig. 12(b) illustrates the gains after loading the lumped capacitors with resistors to drop their Q s to approximately 30. This gives an idea of the effect of loss associated with the capacitors on the system performance. It is obvious from Fig. 12 that the loss degrades the performance of the circuit. In the case of high- Q capacitors, the measured differential-mode gain is 10 dB. However, the common-mode gain is hardly affected and notches at the expected resonant frequency to -10 dB. In the case of low- Q capacitors, the common-mode gain only notches to 0 dB and the differential gain reduces from 10 to 9 dB, as expected from the theory. The measured bandwidth in the two cases is 31% of the resonant frequency of 580 MHz, i.e., 1.36 : 1 bandwidth. This demonstrates the effect of loss, as discussed in Section II.

It is also observed from the measured gains of Fig. 12 that the common-mode gain does not notch exactly at the center of the operating band, as was the case without lumped capacitors [see Fig. 11(b)]. This implies that the frequency at which the odd-mode impedance of the balun peaks to a maximum is different from the frequency at which its even-mode impedance is a minimum. This conflict arises due to the addition of lumped capacitors that cause asymmetry in the characteristics of the even- and odd-mode impedances. This may be resolved by fine tuning of the lumped capacitors and optimization of the rest of the circuit elements of the equivalent even- and odd-mode sub-circuits of the balun structure.

IV. CONCLUSION

A new distributed biasing circuit has been introduced that replaces conventional biasing using inductors. The physical structure comprises transmission lines and a pair of identical coupled lines in the form of a Marchand balun. The circuit is inherently discriminatory in behavior against the common-mode signals generally originating as substrate noise. This discrimination yields a finite CMRR. However, the differential-mode gain remains, to a great extent, unaffected by the presence of loss in the biasing circuit over a broad frequency range. Possible implementation of this new biasing scheme either on an RFIC or off-chip in the package will greatly improve the overall system performance and eliminates the low- Q narrow-band spiral inductors. The distributed biasing-circuit parameters are fairly straightforward to calculate utilizing expressions based on filter principals to obtain a class of desired impedance functions. Experimental data has successfully verified the theory behind the usage of the balun as a viable biasing circuit.

REFERENCES

- [1] T. C. Edwards and M. B. Steer, *Foundations of Interconnect and Microstrip Design*, 3 ed. New York: Wiley, 2000, pp. 350–352.
- [2] R. Mongia, I. Bahl, and P. Bhartia, *RF and Microwave Coupled-Line Circuits*. Norwood, MA: Artech House, 1999, pp. 411–435.
- [3] C. W. Tang and C. Y. Chang, "A semi-lumped balun fabricated by low temperature co-fired ceramic," in *IEEE MTT-S Int. Microwave Symp. Dig.*, June 2002, pp. 2201–2204.
- [4] K. S. Ang, Y. C. Leong, and C. H. Lee, "Analysis and design of miniaturized lumped-distributed impedance-transforming baluns," *IEEE Trans. Microwave Theory Tech.*, vol. 51, pp. 1009–1017, Mar. 2003.
- [5] D. M. Pozar, *Microwave Engineering*. New York: Wiley, 1998.
- [6] J. A. G. Malherbe, *Microwave Transmission Line Filters*. Norwood, MA: Artech House, 1980.

- [7] I. Hunter, *Theory and design of microwave filters*. London, U.K.: IEE Press, 2001.
- [8] A. Tombak, J. P. Maria, F. Ayguavives, Z. Jin, G. Stauf, A. Kingon, and A. Mortazawi, "Tunable barium strontium titanate thin film capacitors for RF and microwave applications," *IEEE Microwave Wireless Comp. Lett.*, vol. 12, pp. 3–5, Jan. 2002.



Wael M. Fathelbab (M'03) received the Bachelor of Engineering (B.Eng.) and Doctor of Philosophy (Ph.D.) degrees from the University of Bradford, Bradford, U.K., in 1995, and 1999, respectively.

From 1999 to 2001, he was an RF Engineer with Filtronic Comtek (U.K.) Ltd., where he was involved in the design and development of filters and multiplexers for various cellular base-station applications. He was subsequently involved with the design of novel RF front-end transceivers for the U.K. market with the Mobile Handset Division,

NEC Technologies (U.K.) Ltd. He is currently a Post-Doctoral Fellow with the Department of Electrical and Computer Engineering, North Carolina State University, Raleigh. His research interests include network filter theory, synthesis of passive and tunable devices, and the design of broad-band matching networks.



Michael B. Steer (S'76–M'82–SM'90–F'99) received the B.E. and Ph.D. degrees in electrical engineering from the University of Queensland, Brisbane, Australia, in 1976 and 1983, respectively.

He is currently a Professor with the Department of Electrical and Computer Engineering, North Carolina State University, Raleigh. In 1999 and 2000, he was a Professor with the School of Electronic and Electrical Engineering, The University of Leeds, where he held the Chair in microwave and millimeter-wave electronics. He was also Director

of the Institute of Microwaves and Photonics, The University of Leeds. He has authored over 260 publications on topics related to RF, microwave and millimeter-wave systems, high-speed digital design, and RF and microwave design methodology and circuit simulation. He coauthored *Foundations of Interconnect and Microstrip Design* (New York: Wiley, 2000).

Prof. Steer is active in the IEEE Microwave Theory and Techniques Society (IEEE MTT-S). In 1997, he was secretary of the IEEE MTT-S. From 1998 to 2000, he was an elected member of its Administrative Committee. He is the Editor-In-Chief of the IEEE TRANSACTIONS ON MICROWAVE THEORY AND TECHNIQUES (2003–2006). He was a 1987 Presidential Young Investigator (USA). In 1994 and 1996, he was the recipient of the Bronze Medallion presented by the Army Research Office for "Outstanding Scientific Accomplishment." He was also the recipient of the 2003 Alcoa Foundation Distinguished Research Award presented by North Carolina State University.